

XENON10/100 dark matter constraints: examining the \mathcal{L}_{eff} dependence

Christopher SAVAGE^{*†}

Stockholm University

E-mail: savage@fysik.su.se

The determination of dark matter constraints from liquid xenon direct detection experiments depends upon the amount of scintillation light produced by nuclear recoils in the detector, a quantity that is characterized by the scintillation efficiency factor \mathcal{L}_{eff} . We examine how uncertainties in the measurements of \mathcal{L}_{eff} and the extrapolated behavior of \mathcal{L}_{eff} at low recoil energies (where measurements do not exist) affect the constraints from experiments such as XENON10 and XENON100, particularly in the light WIMP regions of interest for the DAMA and CoGeNT experimental results.

Identification of Dark Matter 2010

July 26 - 30 2010

University of Montpellier 2, Montpellier, France

^{*}Speaker.

[†]Based on work done in collaboration with Katherine Freese, Graciela Gelmini, and Paolo Gondolo.

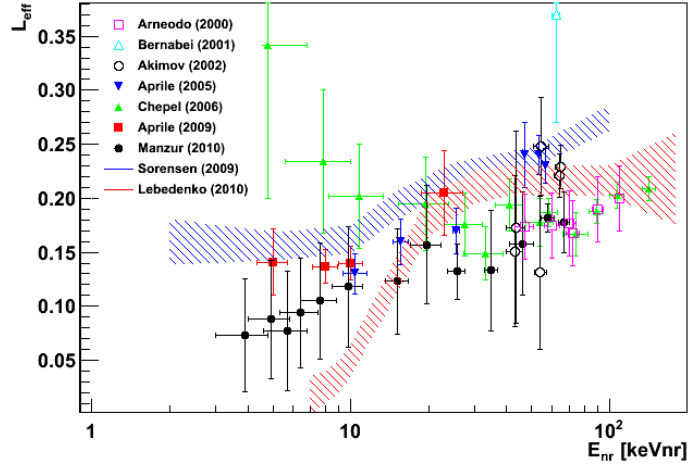


Figure 1: Various measurements of the scintillation efficiency factor \mathcal{L}_{eff} . Figure courtesy of M. Schumann.

1. Introduction

The DAMA annual modulation [1, 2] and the excess low-energy events in CoGeNT [3] can be explained by recoils from a light Weakly Interacting Massive Particle (WIMP); see *e.g.* Ref. [4]. The dark matter interpretation of these signals can potentially be confirmed or refuted by experiments such as XENON10 [5] and XENON100 [6, 7], but the ability of these experiments to probe light WIMPs is dependent on their sensitivity to low energy recoil events in their detectors. The calibration of these detectors' energy scales (and thus knowledge of their sensitivity to low-energy events) is dependent upon the scintillation efficiency factor \mathcal{L}_{eff} . We examine here how the XENON constraints depend upon various models for the poorly known \mathcal{L}_{eff} .

Some of the work presented here is described in Ref. [8], although the analysis of the XENON10 results has been extended down to lower recoil energies with a more careful treatment [9].

2. The \mathcal{L}_{eff} Scintillation Efficiency Factor

Recoils in the XENON detectors produce two scintillation signals, referred to as $S1$ and $S2$, resulting respectively from prompt photons and ionization produced by the collision of a WIMP with a xenon nucleus. Interpretation of the XENON results requires the ability to reliably reconstruct the nuclear recoil energy E_{nr} from the observed $S1$ signal. Calibration of the nuclear recoil energy dependence of $S1$ often involves gauging the detector's response to electron recoils at higher energies; parts of the detector's response (*e.g.* the fraction of scintillation photons that yield photoelectrons (PE) in the photodetectors) are more easily determined in this case than with nuclear recoils at lower energies. Taking $S1$ to be normalized to the number of PE, $S1$ and E_{nr} are related by an equation involving the higher energy electron recoil calibrations:

$$\langle S1 \rangle = (S_{nr}/S_{ee}) \mathcal{L}_{\text{eff}}(E_{nr}) L_{\gamma} E_{nr}. \quad (2.1)$$

Here, L_{γ} is the light yield in PE/keVee for 122 keV γ -rays. $\mathcal{L}_{\text{eff}}(E_{nr})$ is the scintillation efficiency of nuclear recoils relative to 122 keV γ -rays in zero electric field; this factor is a function of the

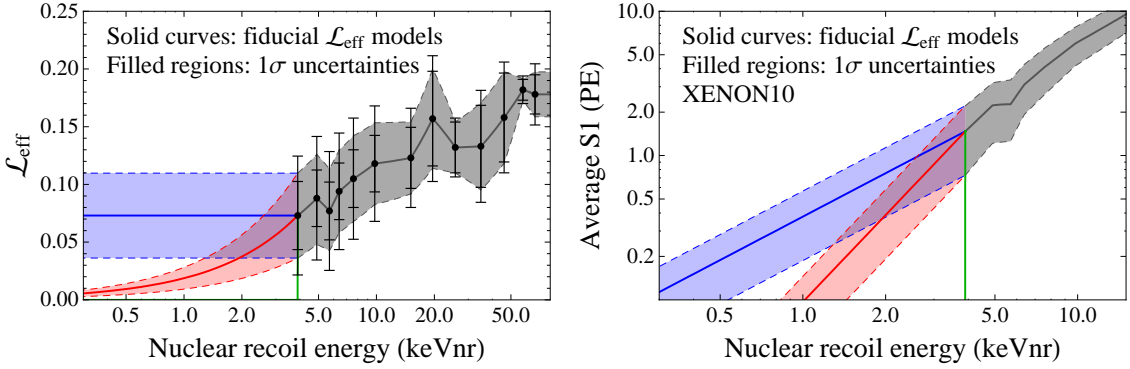


Figure 2: (left) Assumed models for \mathcal{L}_{eff} , based on the Manzur *et al.* measurements [11] with three different extrapolations below $E_{nr} = 3.9$ keV: constant (blue), linearly falling (red), and zero (green). Solid curves indicate fiducial cases, while lighter regions indicate 1σ uncertainties. (right) The expected average S1 signals in XENON10 for these \mathcal{L}_{eff} models. XENON100 exhibits a similar (but not identical) behavior.

nuclear recoil energy. Since there is an applied electric field in the experiment, which reduces the scintillation yield by quickly removing charged particles from the original interaction region, two additional factors must be taken into account: S_{ee} and S_{nr} are the suppression in the scintillation yield for electronic and nuclear recoils, respectively, due to the presence of the electric field in the detector volume. The quantities S_{ee} , S_{nr} , and L_y are detector dependent; \mathcal{L}_{eff} is not. Equation (2.1) describes the *average* S1 signal ($\langle S1 \rangle$); the actual observed S1 signals exhibits some random fluctuations about this average as described in Section 3.

A variety of \mathcal{L}_{eff} measurements and estimates are shown in Figure 1. These measurements are plagued by systematic issues and give conflicting estimates of \mathcal{L}_{eff} at low recoil energies; see Ref. [10] for a discussion regarding the various issues in these \mathcal{L}_{eff} measurements. There are two issues here: (1) Which of the \mathcal{L}_{eff} measurements should be used as a basis for analyzing direct detection results? and (2) Measurements of \mathcal{L}_{eff} have only been made at energies above some minimum; what is the behavior of \mathcal{L}_{eff} at low energies, where no measurements have as yet been made? We do not address the first issue (which set of measurements to use) and simply choose the set of fixed-energy measurements that will give the most conservative constraints: the Manzur *et al.* measurements [11, 12] (black points). For the second issue (the behavior of \mathcal{L}_{eff} at energies below the existing measurements), we consider three extrapolations of \mathcal{L}_{eff} below recoil energies of 3.9 keV (the lowest Manzur measurement): (1) \mathcal{L}_{eff} is constant, (2) \mathcal{L}_{eff} is linearly falling with recoil energy, and (3) \mathcal{L}_{eff} is strictly zero. The XENON estimates of \mathcal{L}_{eff} have been suggestive of the first (constant) case, while the Manzur measurements are more suggestive of the second (falling) case. The third case leads to the most conservative possible constraints by simply ignoring any contributions from recoils with energies below 3.9 keV and is not necessarily a realistic model of the low-energy \mathcal{L}_{eff} behavior. In addition to the dependence of the XENON constraints on these low-energy extrapolations, we consider how the constraints vary within the 1σ uncertainties in the Manzur measurements. Our \mathcal{L}_{eff} models are shown in the left panel of Figure 2, while the right panel of the figure shows the corresponding average S1 signals in the XENON10 detector.

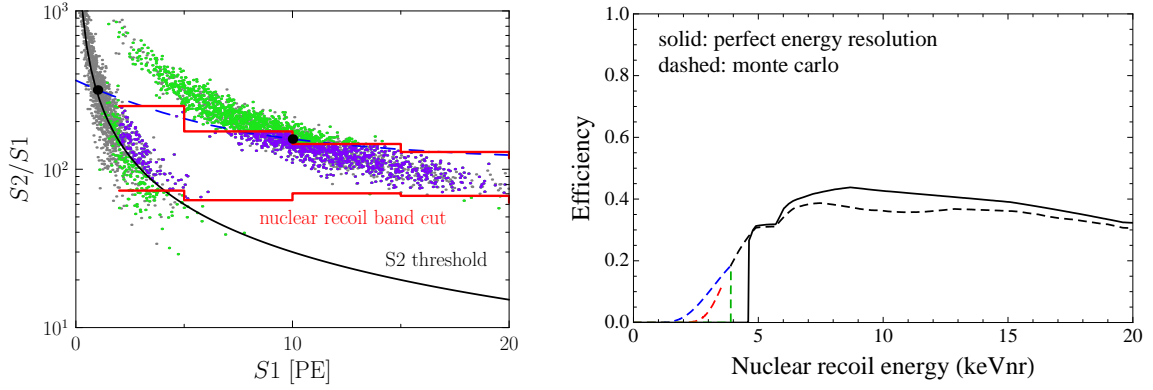


Figure 3: (left) Monte carloed events in the XENON10 detector for nuclear recoils with energies that correspond to average $S1$ signals ($\langle S1 \rangle$) of 1.0 and 10.0 PE (black dots). Events that fail to be identified via the $S1$ peak finding process are shown in gray. Events that are identified but fall either below the $S2$ threshold (black curve) or outside the nuclear recoil band cut (red curves) are shown in green. Events that are identified and pass all cuts (signal events) are shown in purple. (right) The fraction of events at each recoil energy that will be identified and pass all cuts in XENON10 ($2 \leq S1 \leq 75$ PE). The three colored curves at low energies correspond to the three low-energy \mathcal{L}_{eff} extrapolations shown in Figure 2.

3. Detection in XENON10/100

The standard analysis of XENON10 and XENON100 results uses the two scintillation signals $S1$ and $S2$. Due to various physical processes and detector limitations, the observed signals exhibit random fluctuations about the average expected values at a given nuclear recoil energy. The most significant (but not only significant) contribution to the fluctuations is the Poisson fluctuations in the small number of PE's produced by the prompt scintillation (only $\sim 10\%$ of the prompt photons yield a PE), which leads to a poor energy resolution at low recoil energies. We show in the left panel of Figure 3 a monte carlo example of the scattering of the observed $S1$ and $S2$ scintillation signals in XENON10 for recoil energies yielding an average $S1$ of 1.0 and 10.0 PE. We also show the two main cuts—an $S2$ threshold and the nuclear recoil band cut—and take into account the two-fold PMT detection efficiency (also known as the $S1$ peak finding efficiency factor η_{S1}). We use the low-threshold ($S1 \geq 2.0$ PE) XENON10 results of Ref. [5] in our analysis (see also Ref. [13] for a detailed description of the XENON10 detector). We stress that this is a threshold in $S1$, *not* in $\langle S1 \rangle$: as shown in Figure 3, a significant number of events produced at a recoil energy yielding $\langle S1 \rangle = 1.0$ PE will have an observed $S1 \geq 2.0$ PE and pass all cuts, so low-energy recoils can still contribute to the signal within the XENON10 analysis region. To determine the contribution of these low-energy recoils in XENON10, we monte carlo a large number of events at each recoil energy and determine the fraction of events that will be both observed and pass all cuts [9]; the results are shown in the right panel of Figure 3. See Ref. [14] for further discussion regarding the fluctuations of the signals in XENON10 and issues in determining the detection efficiencies.

XENON100 has a lower background than XENON10, but has a higher threshold of $S1 \geq 4$ PE [6, 7]. As the full details of the various data cuts in XENON100 are not yet available, we use for this experiment a simpler model of the efficiency and impose a $\langle S1 \rangle \geq 1.0$ PE cutoff as described in Ref. [8].

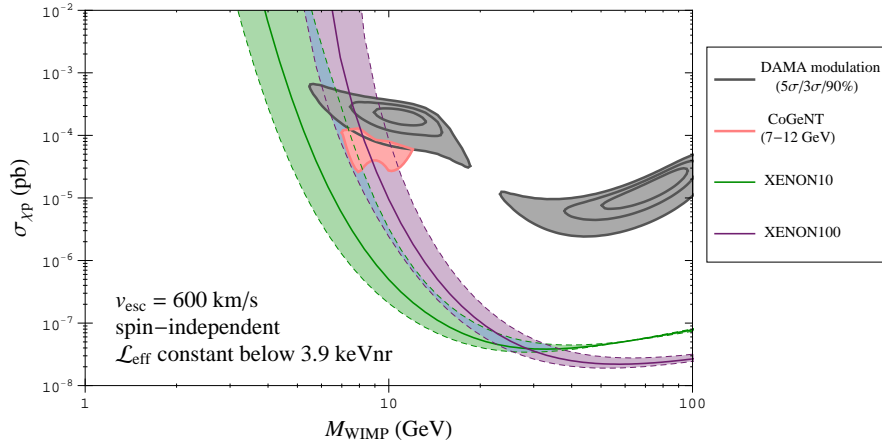


Figure 4: XENON10 (green) and XENON100 (purple) 90% C.L. exclusion constraints for a constant \mathcal{L}_{eff} at recoil energies below 3.9 keVnr. The solid curves are the constraints using the central values of \mathcal{L}_{eff} ; dashed curves and lighter filled regions indicate how these 90% constraints vary with the 1σ uncertainties in \mathcal{L}_{eff} . Overlapping XENON10 and XENON100 regions are shown in blue. Also shown are the DAMA modulation 90%/3 σ /5 σ -compatible regions (gray contours/region) and the CoGeNT 90%-compatible region (pink contour/region over 7-12 GeV).

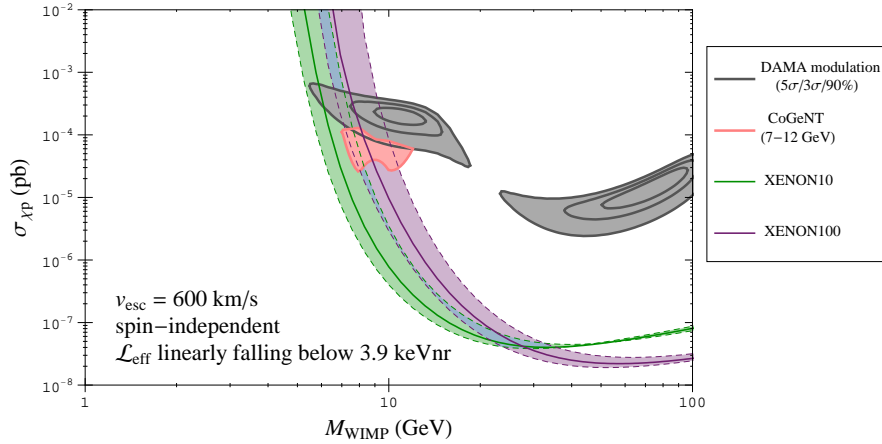


Figure 5: Same as Figure 4, but taking \mathcal{L}_{eff} to fall linearly to zero for recoil energies below 3.9 keVnr.

4. Results and Discussion

We now examine how the XENON10/100 WIMP mass & cross-section constraints are affected by the \mathcal{L}_{eff} model. We consider only spin-independent elastic scattering and assume an isothermal halo model as described in Ref. [8]. The results discussed below apply only to this case; spin-dependent couplings and alternate halo models may affect the compatibility of various experimental results.

Our main results are shown in Figs. 4-6, corresponding to the three cases for the behavior

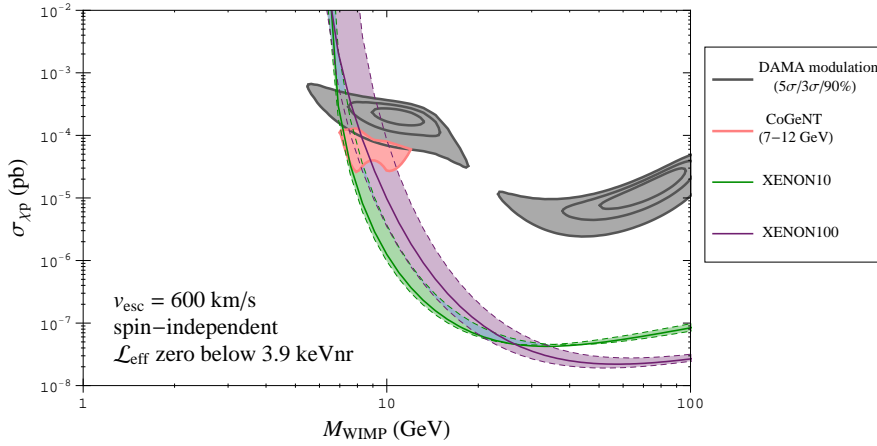


Figure 6: Same as Figure 4, but taking \mathcal{L}_{eff} to be zero for recoil energies below 3.9 keVnr.

of \mathcal{L}_{eff} at low recoil energies. The 90% confidence level (CL) exclusion limits for the fiducial (central) \mathcal{L}_{eff} models are shown as solid curves for XENON10 (green) and XENON100 (purple); lighter filled regions correspond to how these 90% CL exclusion curves vary with the 1σ uncertainty bands in the \mathcal{L}_{eff} models. For comparison, we also show the WIMP parameters compatible with the DAMA modulation [1, 8] (gray contours/regions, corresponding to compatibility within the 5σ , 3σ , and 90% CLs) and the region suggested by CoGeNT [3] (pink contour/region, corresponding to compatibility within the 90% CL).

The XENON100 constraints are nearly identical for all three \mathcal{L}_{eff} models. For the fiducial cases, XENON100 excludes all of the DAMA 3σ region, indicating significant incompatibility between these two experimental results for this dark matter model. XENON100 excludes only the 9-12 GeV WIMP mass part of the CoGeNT region, allowing for 7-9 GeV WIMPs. When the 1σ variations in the Manzur data are considered, however, XENON100 can exclude as little as only the DAMA 90% CL region and almost none of the CoGeNT 90% region to as much as nearly all of the DAMA 5σ CL and CoGeNT 90% CL regions. The similarity of the XENON100 constraints for the different \mathcal{L}_{eff} models is due to the 4 PE threshold: at recoil energies below 3.9 keV, where the models differ, ~ 1 or less PE are expected on average, so recoils at these energies are unimportant.

Due to the lower threshold of 2 PE, the XENON10 constraints are more dependent on the \mathcal{L}_{eff} model. The XENON10 constraints for the three fiducial \mathcal{L}_{eff} cases vary significantly, with the low WIMP mass cut-off varying between ~ 4 GeV and ~ 7 GeV. In all three cases, though, the XENON10 constraints exclude the entire CoGeNT 90% CL and DAMA 3σ CL regions. Though the average $S1$ signal is below threshold for recoil energies below 3.9 keV (where the \mathcal{L}_{eff} models differ), the random fluctuations in the $S1$ and $S2$ signals lead to some events at lower recoil energies being observed above the threshold. For the light WIMPs in the region of interest for DAMA and CoGeNT, the number of low-energy recoils is very large and, even if the fluctuations are small, a significant number of events should still be observed above threshold. If the 1σ bands on \mathcal{L}_{eff} are taken into account, XENON10 still excludes all of the DAMA 3σ region and all but a narrow band of the CoGeNT region over WIMP masses of 7-9 GeV.

While the ability of the XENON dual-signal ($S1$ and $S2$) analyses to constrain light WIMPs is particularly sensitive to systematic issues such as the behavior of \mathcal{L}_{eff} , we note that this type of analysis is optimized more for heavier WIMPs. An analysis based on only the $S2$ signal, such as presented by P. Sorensen in this conference [15], provides much greater sensitivity to light WIMPs. However, we have shown here that the standard dual-signal analysis can still provide stringent constraints on low mass WIMPs even for conservative models of \mathcal{L}_{eff} .

Acknowledgments

C.S. is grateful for financial support from the Swedish Research Council (VR) through the Oskar Klein Centre and thanks his collaborators Katherine Freese, Graciela Gelmini, and Paolo Gondolo. We also thank A. Manalaysay, G. Plante, and P. Sorensen for useful discussions.

References

- [1] R. Bernabei *et al.*, Eur. Phys. J. C **67**, 39 (2010) [arXiv:1002.1028 [astro-ph.GA]].
- [2] P. Belli *et al.* [DAMA Collaboration], in these proceedings.
- [3] C. E. Aalseth *et al.* [CoGeNT collaboration], arXiv:1002.4703 [astro-ph.CO].
- [4] D. Hooper, J. I. Collar, J. Hall and D. McKinsey, arXiv:1007.1005 [hep-ph].
- [5] J. Angle *et al.* [XENON10 Collaboration], Phys. Rev. D **80**, 115005 (2009) [arXiv:0910.3698 [astro-ph.CO]].
- [6] E. Aprile *et al.* [XENON100 Collaboration], arXiv:1005.0380 [astro-ph.CO].
- [7] M. Schumann *et al.* [XENON100 Collaboration], in these proceedings.
- [8] C. Savage, G. Gelmini, P. Gondolo and K. Freese, arXiv:1006.0972 [astro-ph.CO].
- [9] C. Savage, G. Gelmini, P. Gondolo and K. Freese, in preparation.
- [10] A. Manalaysay, arXiv:1007.3746 [astro-ph.IM].
- [11] A. Manzur, A. Curioni, L. Kastens, D. N. McKinsey, K. Ni and T. Wongjirad, Phys. Rev. C **81**, 025808 (2010) [arXiv:0909.1063 [physics.ins-det]].
- [12] D. McKinsey, in these proceedings.
- [13] E. Aprile *et al.* [XENON Collaboration], arXiv:1001.2834 [astro-ph.IM].
- [14] P. Sorensen, arXiv:1007.3549 [astro-ph.IM].
- [15] P. Sorensen *et al.*, in these proceedings [arXiv:1011.6439 [astro-ph.IM]].